

Efficiency Gain For Bi-Facial Multi-Crystalline Solar Cell With Uncapped Al_2O_3 And Local Firing-Through Al-BSF

Ilkay Cesar¹, Petra Manshanden¹, Gaby Janssen¹, Ernst Granneman², Olga Siarheyeva²,
and Arthur W. Weeber¹

1) ECN Solar Energy, P.O. Box 1, 1755 ZG Petten, The Netherlands, corresponding author:
cesar@ecn.nl

2) Levitech BV, Versterkerstraat 10, 1322 AP Almere, The Netherlands

Abstract — The p-type bi-facial cell concept, p-PASHA (Passivated on all sides H- pattern), is developed at ECN and employs an uncapped Al_2O_3 passivation layer on the rear through which a screen printed H-pattern of aluminium contacts is fired. Here we report a net gain in cell efficiency of 0.2% absolute for the p-PASHA cell vs. industrial reference with the addition of a clean and an ALD step. Even higher gains up to 0.5% abs. are expected after optimization of the cell design and process. Apart from the efficiency gain, the bi-facial cell concept allows for 50-80% reduction in Al paste consumption, the use of thinner wafers, and consists of less processing steps compared to prevalent PERC concepts. The Al_2O_3 dielectric layer is deposited in the Levitrack, an industrial-type system for high-throughput Atomic Layer Deposition (ALD) developed by Levitech. The efficiency gain is obtained on multi-crystalline wafers, at a rear metal fraction of 40%. Localized IQE mapping, cross-sectional SEM investigation, resistance measurements and 2D simulation relate the efficiency improvement compared to our conventional process to better eutectic and BSF formation at the Al contact edges.

Index Terms — Bi-facial, p-type, Al_2O_3 , ALD, firing-through, Al-BSF, multi-crystalline, eutectic.

I. INTRODUCTION

In order to process thinner wafers at an increased cell efficiency, the conventional full Al rear side of p-type solar cells can be replaced by an open rear metallization combined with a dielectric passivation layer. This cell concept is referred to as the PASHA cell (Passivated on all sides H- pattern) and is illustrated in Fig. 1. For this rear passivated multi-crystalline solar cell with local contacts, we estimate that the bi-facial cell could result in a gain of 0.5% in absolute efficiency [1]. This gain can be achieved when the bi-facial cell is placed on an effective rear reflector such as a (module) back-sheet foil, optimized for reflections between 1000 and 1300 nm as the transmittance in this range increases as the wafer thickness decreases. The principle gain factors in terms of $J_{sc} \times V_{oc}$ are improved effective rear reflection and improved passivation of the dielectric layer as compared to a standard full Al-BSF. This efficiency gain is a balance of the superior passivation and reflection quality of the dielectric layer compared to the metal contacts and extra resistive losses in the base and the metal grid that are induced by the openings in the rear metal design. The efficiency gain can be obtained if the local BSF quality of the contacts matches the quality of the full area BSF in combination with SRV values below 10 cm/s

for the dielectric layer. Additional advantages of the bi-facial cell are reduced consumable costs, as the Al-paste use per cell will likely be reduced by 50-80% depending on the optimal metallization design while reduced cell bowing after firing will increase production yield due to less cell breakage.

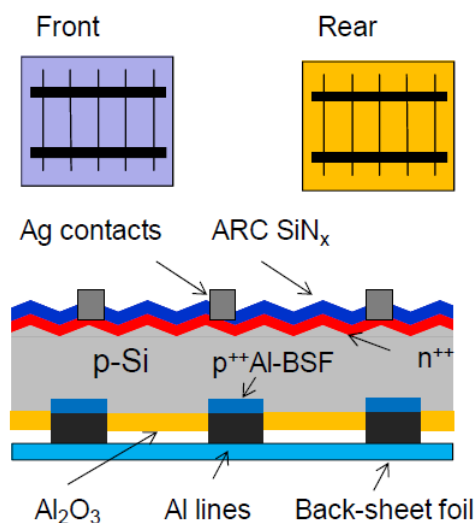


Fig. 1. bi-facial cell concept with metal print on front and rear consisting of parallel fingers connected to busbars. The optimal metal fraction on the rear is expected to lie between 20 and 50%. The back-sheet foil as well as the rear metallization, reflect photons at wavelengths between 1000-1300 nm back into the solar cell.

It is our approach to limit the extra processing steps for the bi-facial cell as compared to for example the prevalent PERC type processing. Usually the PERC process consists of a polishing step, a stack of dielectric layers of substantial combined thickness (~100nm), an opening step and full area Al metallization. In our previous work we have shown a gain of 2.5 % in $J_{sc} \times V_{oc}$ on multi-crystalline material vs. the reference process with a p-PASHA process that included a polishing step, a non-industrial PASHA-clean step. This cell did not show an efficiency gain vs. the reference due to resistive losses in the rear owed to the 2 busbar based metallization design with a metal fraction of 30% [2]. We have further established the long term stability of p-PASHA single cell laminates by successfully passing thermal cycle and

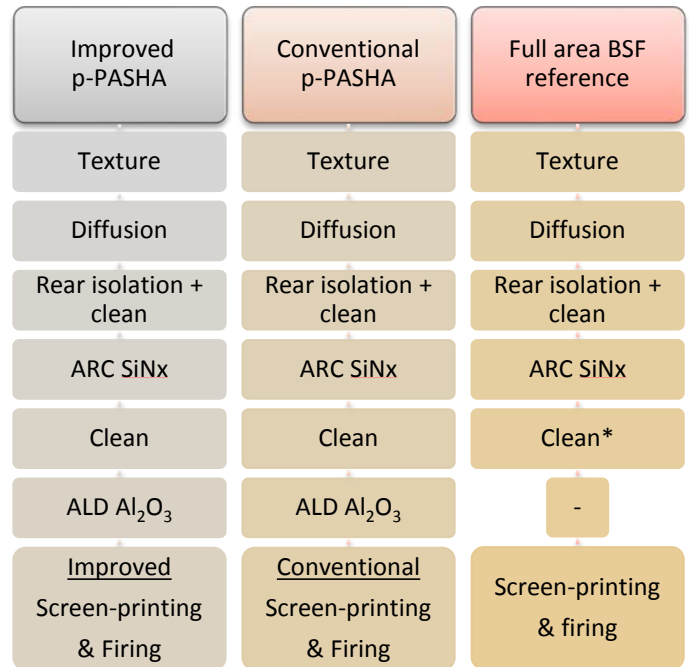
damp heat tests [2]. We have shown that a homogeneous BSF can be formed after firing-through the Al_2O_3 coating alleviating the need for opening the dielectric but also identified the edge of the Al-contact as an important recombination source [2,3]. In this work, we took a step to industrialize our process by omitting the polishing and the PASHA clean and adopted a 3 busbar design with a 40% metallization fraction to reduce resistive losses. This approach resulted in a 0.2 % absolute efficiency gain compared to the Al-BSF reference at the expense of 2 additional process steps. Furthermore, we show experimental and numerical evidence that the formation of an eutectic and BSF up to the edges of the aluminum rear contacts is vital for the obtained efficiency gain.

II. Al_2O_3 PASSIVATION AND LOCAL BSF FORMATION

As a passivating dielectric, aluminum oxide has received much attention in recent years because of its potential surface passivation performance in silicon solar cells [4]. It is known to passivate boron emitters [5] and can be applied as rear dielectric in rear passivated solar cells based on p-type wafers, like the PERC [6] and the PASHA cell [3]. High surface passivation levels of Al_2O_3 layers, expressed by values below 10 cm^2/s for the effective surface recombination velocity S_{eff} , are commonly reported. The reduced recombination at the surface is caused by field effect as well as chemical passivation. This dielectric is characterized by very high negative surface charge density ($10^{12} - 10^{13} \text{ cm}^{-2}$) [7,8] that repels electrons from the surface, reducing the chance for holes to recombine. A major advantage of the negatively charged Al_2O_3 on p-type surfaces is that it does not cause inversion layer shunting. This phenomenon severely reduces the J_{sc} of rear passivated solar cells and is commonly observed for positively charged dielectrics such as SiN_x [9,10]. Although Al_2O_3 has proven its potential as effective rear dielectric in high-efficiency solar cells (> 20%) [6], its application in industry is impeded by several factors: 1) low wafer throughput rates related to the deposition method and lengthy anneals, 2) firing stability and 3) contact formation through the dielectric. These issues are addressed in this work. Benick et al. studied the surface recombination velocity of 27 nm thick Al_2O_3 layers deposited on p-Fz (1 $\text{ohm}\cdot\text{cm}$) by Plasma Enhanced ALD [5]. It is reported that the SRV increased from below 10 cm^2/s at a peak temperature of 700°C to values well above 1000 cm^2/s at 850°C[5].

Screen printable Al pastes can enable the formation of a localized BSF when firing through Al_2O_3 passivation layers. The peak firing temperature is known to be an important factor for both the BSF dopant density and thickness [11]. Therefore, higher peak temperatures are expected to yield a thicker localized BSF under the Al grid lines. Thus, the main challenge for the industrialization of the Al_2O_3 passivating layer and the firing-through paste is to optimize the BSF formation to match the firing condition at which the Al_2O_3

retains its passivation quality. Measures to improve the firing stability by capping the Al_2O_3 layer, as well as the application



of long forming gas anneals steps, are unfavorable for industrialization.

Fig. 2. Process flows for improved and conventional p-Pasha, and an industrial reference p-type process are compared. The clean* after the ARC in the reference group is included for fair comparison with p-PASHA groups.

III. PROCESS FLOW

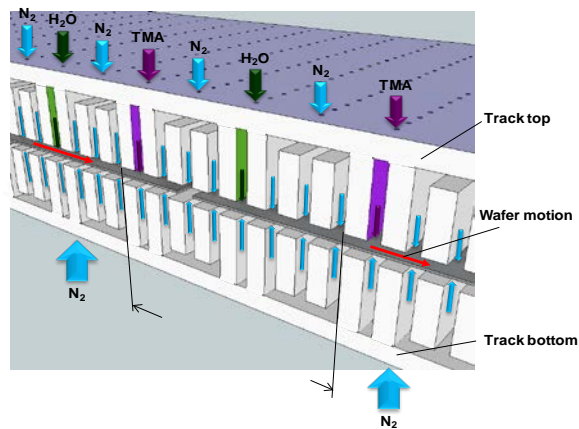
The potential for industrial rear side passivation of uncapped Al_2O_3 layers was assessed on 6 inch p-type multi crystalline wafers (sister wafers). The wafers were textured on the front and rear side. They received a 75 ohm/sq emitter (tube furnace using POCl_3), followed by a chemical isolation step. After the ARC layer deposition (SiN_x PECVD), all groups received the same industrial clean steps to ensure the same ARC properties. The wafers were coated with a layer of Al_2O_3 on the rear using our in-house the Levitrack ALD system. Subsequently a three busbar based metallization grid was printed and fired using Al firing-through paste on the rear and Ag paste on the front. These cells had a rear metal fraction of 40%. We report on two p-PASHA groups with differences in the metallization and the firing which will be referred to as the conventional and the improved p-PASHA process. The complete process flow is shown in Fig. 2

The samples are characterized by means of IV, LBIC, SEM and spectral response. In order to measure the FF most

representative for the module interconnection, the rear is contacted only at the busbars during the IV measurement allowing a voltage drop to occur in the rear fingers. To mimic the IR reflectance of the backsheet foil in a module, all IV, IQE and reflectance measurements were conducted with a rear reflector in air. In order to expose the BSF in the SEM images, samples have been broken along a groove that was laser scribed perpendicularly to the fingers on the sunny side of the p-PASHA cell. A stain etch has been performed that selectively etches the BSF.

IV. LEVITRACK: HIGH THROUGHPUT ALD OF Al_2O_3

In conventional ALD of Al_2O_3 the precursors TMA and H_2O are sequentially injected into a low-pressure reaction chamber, separated (in time) by inert gas (N_2) purges. In a complete ALD cycle (TMA, N_2 , H_2O , N_2), the layer thickness increases with $\sim 0.09\text{-}0.12$ nm/cycle, depending on the process temperature. Films are grown at low temperatures ($150\text{-}300^\circ\text{C}$) with excellent step coverage and almost ideal morphology. Unfortunately, one of the drawbacks of the conventional ALD method is the low throughput, typically 50 wafers/hr. This is far too low to be of interest for the PV industry where throughputs in the range of 2400 wafers/hr are required.



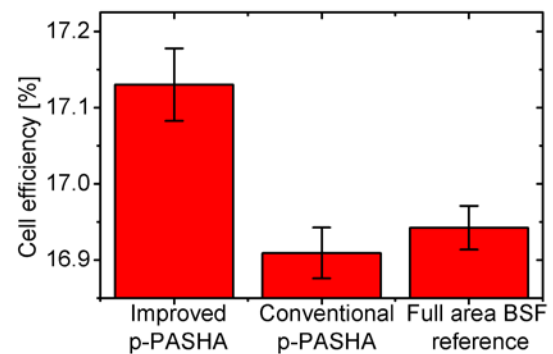
a)



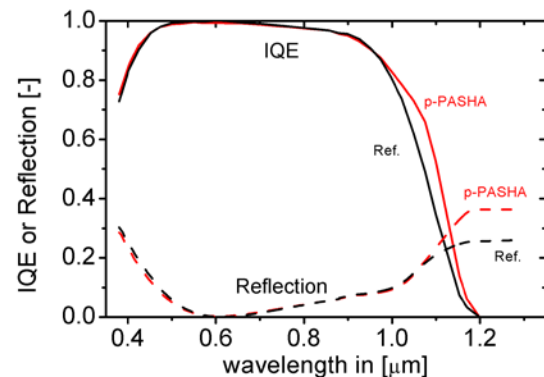
b)

Fig. 3. Layout of the Levitrack ALD system for Al_2O_3 layers. Fig. a) shows a schematic cross section of the Levitrack. b) Photograph of the Levitrack ALD system.

In the Levitrack, sketched in Fig. 3, wafers are transported in a linear track. During the process, the wafers are floating on a gas bearing. The gas bearing ensures that during the entire process there is no physical contact with the track walls. The combination of a gravitational force and viscous drag ensures a constant transport velocity of the wafers through the track. During transport the wafers pass several segments in which they are sequentially, single-sidedly exposed to TMA, N_2 , H_2O and N_2 ; a so-called ALD cell. The system contains many of such ALD cells, each of which has a typical length of 12 cm and can be switched on and off for Al_2O_3 layer thickness tuning; in each of these cells 0.12 nm aluminum oxide is deposited. With the Levitrack system, single sided Al_2O_3 layers can be deposited at a throughput of up to 3600 wafers/hr. The non-uniformity is in the range of 3% 1sigma% with a non-reproducibility $<1\%$



a)



b)

Fig. 5. Cell efficiencies (a), IQE and reflection spectra (b) of the multi-crystalline p-PASHA (red) cell compared to an full Aluminum BSF reference (black). The error bars in (a) are from the statistical Tukey HSD analysis.

VI. CELL AND LBIC RESULTS

In direct comparison on neighbor material with the full area BSF reference, the p-PASHA cell showed a 0.2% gain in efficiency as shown in Fig. 5a. The largest improvement as compared to the full area BSF reference is observed in J_{sc} as seen from Table 1, which is attributed to improved internal reflection of the rear of the p-PASHA cell as illustrated in the IQE and Reflection spectra in figure 5b. The efficiency gain is obtained after improvement of the metallization and firing process of the p-PASHA cell. The improved process increased the J_{sc} , V_{oc} and FF of the p-PASHA cell.

Table 1. The multi-factor ANOVA analysis comparing IV parameters of multi-crystalline p-PASHA cells with that of the reference. The relative standard error is reported in parentheses.

Cell	J_{sc} [mA/cm ²]	V_{oc} [V]	FF [%]	Eta [%]
Improved p-PASHA	35.5 (0.18%)	0.616 (0.14%)	78.3 (0.12%)	17.1 (0.28%)
Conventional p-PASHA	35.4 (0.18%)	0.613 (0.14%)	78.0 (0.12%)	16.9 (0.28%)
Full area BSF ref.	34.9 (0.11%)	0.618 (0.08%)	78.6 (0.07%)	16.9 (0.17%)

The IQE spectra of the Al-BSF and the improved p-PASHA cell, shown in Fig. 5b, overlap in the blue and the visible red, while distinct difference are measured in the IR

above 950 nm. The improvement is related to a higher apparent internal reflection coefficient for the p-PASHA cell which affect photons that interact with the rear Si surface and the rear reflector at wavelengths above 950 nm as discussed previously [1]. The higher internal reflection on the rear usually also increases the escape reflectance at wavelengths above 1100 nm which corroborates with the measured reflection spectra of both cell types. The fact that the IQE spectra overlap below 950 nm indicates that the net passivation of the Al-BSF and the p-PASHA are on par. The IQE and reflection spectra of the conventionally processed p-PASHA cell (not shown) is nearly identical to that of the improved cell which is reflected in the small differences in J_{sc} .

The improvement in cell performance between the conventional and improved p-PASHA process is reflected in the LBIC mappings measured at 976 nm as seen in Fig. 6. For the conventional process, the edges of the rear aluminum contacts are clearly visible by the local drop in IQE while the edge feature nearly vanishes for the improved process. The cross-sectional SEM images in Fig. 6 confirm that BSF extends further to the edges of the contact which reduces the area of unshielded contacts and should increase both J_{sc} and V_{oc} . The influence of the unshielded edge on the V_{oc} will be discussed in paragraph VII. Interestingly also the FF increased for the cell prepared by the improved process which can be attributed to lower Al line resistances as measured with busbar-to-busbar resistance measurements. As the eutectic layer consist for 88% of aluminum, it contributes strongly to the conductance of the rear finger [12]. The SEM images

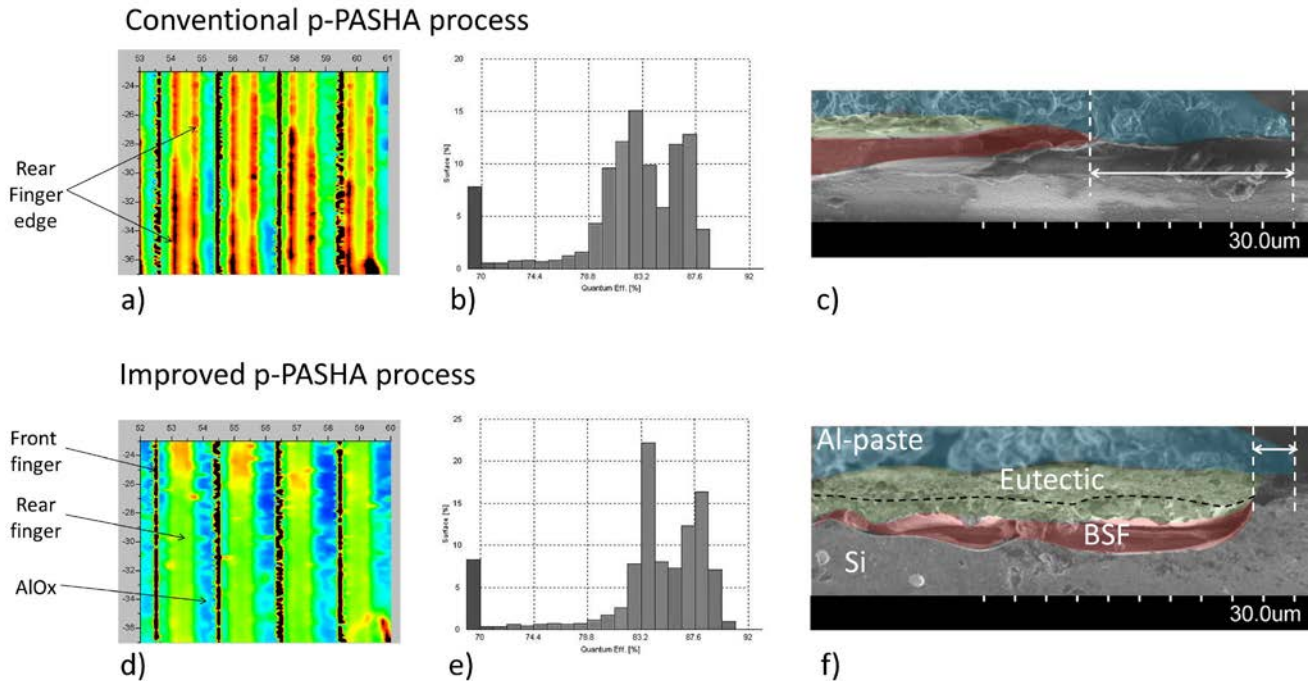


Fig. 6. Comparison of conventional and improved p-PASHA process: (a, d) Laser beam induced current IQE mapping (range 70 to 92%) at a wavelength of 976 nm. Illumination is done through the emitter; silver fingers appear in black; (b,e) histograms of the IQE mappings; (c, f) SEM cross-section of BSF and eutectic formation near the aluminum contact edge on the rear of the p-PASHA solar cell. Coloration is added to guide the eye and indicate paste (blue), green (eutectic) and (red) BSF. The black dashed line in image f) marks the edge of the eutectic layer.

show that the eutectic is wider for the improved process increasing the width of the most conductive part of the finger.

VII. NUMERICAL SIMULATIONS

A. Details of the simulations

Numerical simulations were carried out to investigate the effect of unshielded metal area on the open circuit voltage V_{oc} . This comprised both the effect of the total unshielded metal area and the distribution of this area over the rear side.

The simulations were done using the Atlas package [13] on a 2D unit cell which had the width of a half the front side pitch. At the rear side either one or two metal fingers were included in the unit cell. This means that at the rear the pitch was taken either equal to the front-side pitch or reduced by 50%. The frontside pitch was set to 2 mm, i.e. the unit cells had a width of 1 mm. Fig. 7 shows a schematic outline of the two unit cells studied.

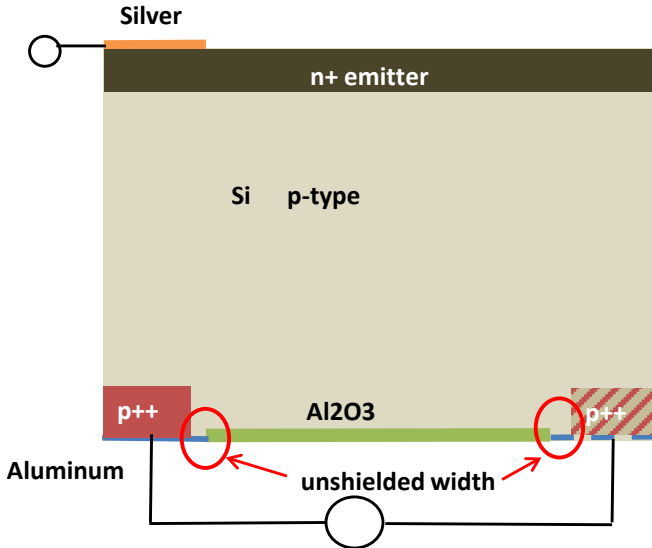


Fig. 7. Schematics of the structures used for the simulations. The width of the unshielded metal was varied. The full width of both structures was 1 mm.

The presence of unshielded metal at the rear was modeled by letting the width of the Al+BSF be smaller than the Al metal width. The width of this unshielded metal was varied between 0 and 40 μm per contact edge. The BSF profile had a depth of 6 μm , no roll-off effects were assumed at the edges of the BSF. The rear metal fraction was 40% and a good surface passivation was assumed for the Al_2O_3 covered surface, i.e. with surface recombination velocities $S_n=S_p=10 \text{ cm s}^{-1}$.

The parameterization of the properties of the substrate, emitter and emitter surface was chosen such that the V_{oc} of a cell with a full width BSF and metal was 619 mV.

B. Results and discussion

Fig. 8 shows that the reduction from 100% Al coverage metal surface to 40% metal coverage results in a gain in V_{oc} of 14 mV for fully shielded contacts. This of course reflects the good passivation assumed for the rear $\text{Si}/\text{Al}_2\text{O}_3$ interface.

The presence of unshielded contacts counteracts this gain, as Fig. 8 also shows. The reduction of the V_{oc} with unshielded metal width is expected on the basis of simple analytical approach. The V_{oc} of a cell is given by:

$$V_{oc} = \frac{kT}{q} \ln \left(\frac{J_{sc}}{J_0} + 1 \right) \quad (1)$$

The dark saturation current density J_0 of the cell may be approximated by an area weighted average of the J_0 contributions from different areas of the cell .

$$J_0 = J_{0,1} + J_{0,ms} f_{ms} + J_{0,us} f_{us} + J_{0,ox} f_{ox} \quad (2)$$

Here the $J_{0,1}$ refers to contributions of the substrate and the base. The $J_{0,ms}$, $J_{0,us}$ and $J_{0,ox}$ are the J_0 of the shielded metal, the unshielded metal and the oxide interface respectively. The f_i denote the fractions of rear interface that is shielded metal, unshielded metal and oxide. With this approximation the V_{oc} can be written as:

$$V_{oc} = \frac{kT}{q} \left[\ln J_{sc} - \ln \left(J_{0,1} + J_{0,ms} f_{ms} + J_{0,us} f_{us} + J_{0,ox} f_{ox} \right) \right] \quad (3)$$

From (3) it follows that the impact of unshielded metal width will be larger if the other parts of the cell contribute less, i.e. in well optimized cells made from good quality wafers.

The spread in acceptable values at the specified metal fraction of 40%, reflects the simulation result that the decrease in V_{oc} also depends on the rear pitch (i.e. number of rear fingers), as Fig. 8 shows. When the pitch is reduced, the number of fingers increases and this would result in an increase of total unshielded width. However, the curves in Fig. 8 show that the drop in V_{oc} is larger for the reduced-pitch case, even if the total unshielded width would be the same. This shows the limitations of the area weighted J_0 approach used in (2). The decrease in voltage is more pronounced when the unshielded width is more distributed over the rear especially for large unshielded widths.

The results presented here indicate that a width of unshielded metal smaller than 2-4 μm per contact edge can result in a V_{oc} gain compared to the reference cell, provided

the number of rear fingers is not too high (<140). As mentioned above, the edge effect will be more severe for better quality cells. Although reduction of the rear pitch will improve the fill factor, it is also clear that even at the same total unshielded width, this can incur a penalty in V_{oc} of 1-2 mV in the case of the improved p-PASHA process. These results imply that with an unshielded metal width in the order of 1-2 μm per contact edge, the edge effect and its distribution must be taken into account in the optimization of the cell design. Only when the width of unshielded metal is smaller than 100 nm per edge, the impact of edge effects will become less than 3 mV in V_{oc} .

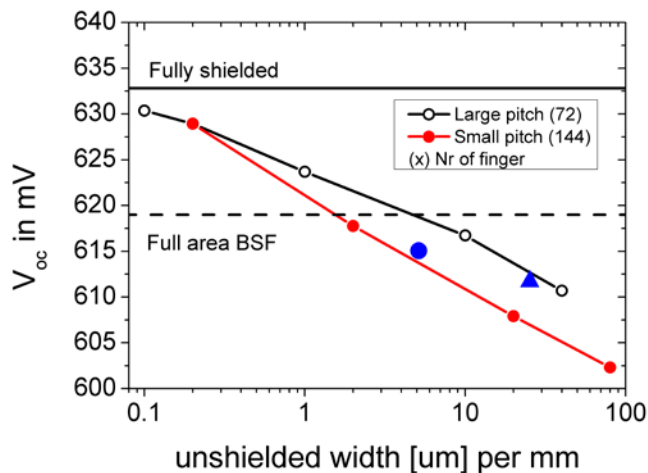


Fig. 8. Calculated V_{oc} values as a function of the total unshielded width per mm cell width at a metal fraction of 40%. Lines are drawn to guide the eye. Blue symbols indicate the experimental values of this work: (triangle) Conventional; (circle) Improved p-PASHA.

VIII. CONCLUSION

The PASHA concept is an attractive concept to improve the cell efficiency of standard full area Al-BSF solar cells by replacing the rear side with a passivated surface and an open aluminum grid. The rear contacts are fired-through an uncapped Al_2O_3 passivation layer deposited in the Levitrack; a high throughput ALD tool. A gain in cell efficiency of 0.2% abs. is obtained for the p-PASHA cell with a 3 busbar design at an aluminum coverage fraction of 40% and at the expense of two additional industrial processing steps compared to the reference process: 1) a clean and 2) the ALD tool. The largest gain was found in J_{sc} and was attributed to a higher apparent internal reflection coefficient on the rear of the bifacial cell when measured with a rear reflector in air, which closely mimics the encapsulated condition in a module. The net gain in cell efficiency for the p-PASHA cell was obtained after improving the BSF and eutectic formation at the aluminum contact edge as was confirmed by 2D simulations. For

unshielded contact edges smaller than 2-4 microns, a gain in V_{oc} is predicted for the p-PASHA cell compared to the reference. Future optimization of the rear metal pattern is likely to yield even higher cell efficiencies.

ACKNOWLEDGEMENT

Agentschap NL is acknowledged for financial support.

REFERENCES

- [1] I. Cesar, E. E. Bende, G. Galbiati, L. Janßen, A.A. Mewe, P. Manshanden, A. W. Weeber, and J. H. Bultman, "Parasitic shunt losses in all-side SiNx passivated mc-Si solar cells" Proc. 24th EUPVSEC 2009.
- [2] I. Cesar, A.A. Mewe, P. Vermont, E. Granneman, A.W. Weeber, "Improved Performance of Uncapped Al_2O_3 and Local Firing-Through Al-BSF in Bi-facial Solar Cells" Proc. 38th IEEE PVSEC, Austin 2012.
- [3] I. Cesar, E. Granneman, P. Vermont, H. Khatri, H. Kerp, A. Shaikh, P. Manshanden, A.A. Mewe, I.G. Romijn, A.W. Weeber, "Industrial Application of Uncapped Al_2O_3 and Firing-Through Al-BSF In Open Rear Passivated Solar Cells" Proc. 37th IEEE PVSEC, Seattle 2011
- [4] G. Dingemans, Nanolayer Surface Passivation Schemes for Silicon Solar Cells. Thesis Eindhoven University of Technology, 2011
- [5] J. Benick, A. Richter, M. Hermle, and S. W. Glunz, Thermal stability of the Al_2O_3 passivation on p-type silicon surfaces for solar cell applications" Phys. Status Solidi RRL, 3, 233 (2009).
- [6] J. Schmidt, A. Merkle, R. Brendel, B. Hoex, M.C.C. van der Sanden, and W. M. M. Kessels, "Surface passivation of high-efficiency silicon solar cells by atomic-layer-deposited Al_2O_3 " Progress in Photovoltaics: Research & Applications, vol. 16, no. 6, pp. 461-466, 2008.
- [7] B. Hoex, J. Schmidt, P. Pohl, M. C. M. van de Sanden, and W. M. M. Kessels, "Silicon surface passivation by atomic layer deposited Al_2O_3 ", J.Appl.Phys., 104, 4, (2008) 044903/1.
- [8] G. Dingemans, M. C. C. van der Sanden, and W. M. M. Kessels, "Influence of the Deposition Temperature on the c-Si Surface Passivation by Al_2O_3 Films Synthesized by ALD and PECVD", Electrochemical and Solid-State Letters, 13, 3 2009, pp. H76-79H.
- [9] S. Dauwe, L. Mittelstadt, A. Metz, and R. Hezel, "Experimental evidence of parasitic shunting in silicon nitride rear surface passivated solar cells", Progress in Photovoltaics Research and Applications, 10, 4, 2002, pp. 271-278.
- [10] I. Cesar, A.A. Mewe, P. Manshanden, I.G. Romijn, L. Janßen, A.W. Weeber, "Effect of Al contact pitch on rear passivated solar cells", Energy Procedia, Volume 8, 2011, Pages 672-680

- [11] J. Krause, R. Woehl, M. Rauer, C. Schmiga, J. Wilde, D. Biro, "Microstructural and electrical properties of different-sized aluminum-alloyed contacts and their layer system on silicon surfaces", *Solar Energy Materials and Solar Cells*, Volume 95, Issue 8, August 2011, Pages 2151-2160
- [12] Atlas, www.silvaco.com